Applied and Environmental Microbiology, Oct. 2007, p. 6241–6253 Vol. 73, No. 19
0099-2240/07/$08.00+0 doi:10.1128/AEM.00977-07
Copyright © 2007, American Society for Microbiology. All Rights Reserved.

Characteristics of *Gloeophyllum trabeum* Alcohol Oxidase, an Extracellular Source of H_2O_2 in Brown Rot Decay of Wood[▽]

Geoffrey Daniel,[1]†* Jindřich Volc,[2]† Lada Filonova,[1] Ondřej Plíhal,[2] Elena Kubátová,[2] and Petr Halada[2]

Department of Forest Products, Swedish University of Agricultural Sciences, P.O. Box 7008, SE-750 07 Uppsala, Sweden,[1] and Institute of Microbiology v.v.i., Academy of Sciences of the Czech Republic, Vídeňská 1083, 142 20 Prague 4, Czech Republic[2]

Received 1 May 2007/Accepted 23 July 2007

A novel alcohol oxidase (AOX) has been purified from mycelial pellets of the wood-degrading basidiomycete *Gloeophyllum trabeum* and characterized as a homooctameric nonglycosylated protein with native and subunit molecular masses of 628 and 72.4 kDa, containing noncovalently bonded flavin adenine dinucleotide. The isolated *AOX* cDNA contained an open reading frame of 1,953 bp translating into a polypeptide of 651 amino acids displaying 51 to 53% identity with other published fungal AOX amino acid sequences. The enzyme catalyzed the oxidation of short-chain primary aliphatic alcohols with a preference for methanol (K_m = 2.3 mM, k_{cat} = 15.6 s^{-1}). Using polyclonal antibodies and immunofluorescence staining, AOX was localized on liquid culture hyphae and extracellular slime in sections from degraded wood and on cotton fibers. Transmission electron microscopy immunogold labeling localized the enzyme in the hyphal periplasmic space and wall and on extracellular tripartite membranes and slime, while there was no labeling of hyphal peroxisomes. AOX was further shown to be associated with membranous or slime structures secreted by hyphae in wood fiber lumina and within the secondary cell walls of degraded wood fibers. The differences in AOX targeting compared to the known yeast peroxisomal localization were traced to a unique C-terminal sequence of the *G. trabeum* oxidase, which is apparently responsible for the protein's different translocation. The extracellular distribution and the enzyme's abundance and preference for methanol, potentially available from the demethylation of lignin, all point to a possible role for AOX as a major source of H_2O_2, a component of Fenton's reagent implicated in the generally accepted mechanisms for brown rot through the production of highly destructive hydroxyl radicals.

The basidiomycete *Gloeophyllum trabeum* is a representative of the brown rot fungi, which are characterized by a special pattern of wood decay during which they oxidatively degrade wood cell wall components, causing a rapid loss of wood strength (18). Brown rot fungi are the principal cause of the highly destructive form of decay observed in wooden constructions, particularly in temperate geographic areas (21). In addition, *G. trabeum* and *Serpula lacrymans* are possibly the most reported fungal species causing wood decay in houses. The molecular mechanisms and enzymatic systems these fungi use during the rapid and selective depolymerization of wood cellulose with incipient decay has been highly debated and researched for many years but remain controversial and not fully understood. In current decay models, a central role for a low-molecular-weight immediate depolymerizing agent that can easily penetrate wood cell walls is ascribed to hydroxyl radicals (·OH) generated nonenzymatically from extracellular H_2O_2 (35, 37, 47). The generally accepted mechanism for ·OH formation during brown rot decay is provided by the Fenton reaction: $H_2O_2 + Fe^{2+} + H^+ \rightarrow {\cdot}OH + Fe^{3+} + H_2O$.

For production of H_2O_2 and regeneration of Fe^{2+}, *G. trabeum* is reported as using extracellular phenolate biochelators (19, 32, 58). Of these biochelators, 2,5-dimethoxyhydroquinone and 4,5-dimethoxycatechol were identified and proposed to play a key role in providing the Fenton reactants via a hydroquinone-quinone redox cycle (30, 32, 41, 45, 50) driven by an intracellular low-specificity NADH quinone reductase (5, 31). H_2O_2 is formed nonenzymatically by dismutation of intermediate ·OOH/$O_2{\cdot}^-$ oxyradicals produced by reduction of O_2 by semiquinones or when either of these radicals are reduced by Fe^{2+} (24). An alternative pathway for Fenton chemistry using the enzyme cellobiose dehydrogenase was suggested for the brown rot fungus *Coniophora puteana* (28). This degradation scheme, however, has not been shown to function with *G. trabeum* (18, 25). Other low-molecular-weight oxidative degrading chemistries proposed for explaining *G. trabeum* decay activities include an extracellular Fe^{3+}-chelating/reducing glycopeptide (13) or peptide (53, 54). However, all of these systems for ·OH generation are notably H_2O_2 dependent.

In view of the Fenton chemistry, we assume that alcohol oxidase (AOX) (EC 1.1.3.13), an H_2O_2-producing enzyme we detected in high levels in cultures of *G. trabeum*, could also play a crucial or supportive role in the decay process, considering the enzyme substrate specificity and high levels of its expression. Although brown rot fungi, in contrast to white rot fungi, have not developed a peroxidase system for extensive lignin degradation, they can during initial stages of decay substantially modify this polymer by efficient demethylation (15, 16), thus producing methanol, a preferred physiological substrate of AOX. Because methanol is unlikely to be of any

* Corresponding author. Mailing address: Department of Forest Products/Wood Science, Swedish University of Agricultural Sciences, P.O. Box 7008, SE-750 07 Uppsala, Sweden. Phone: 46-18672489. Fax: 46-18673489. E-mail: geoffrey.daniel@sprod.slu.se.

† G.D. and J.V. contributed equally to this study.

▽ Published ahead of print on 27 July 2007.

nutritional value for this fungus (in contrast to that known for methanol-utilizing yeasts), we suppose that AOX is more likely related to oxidative wood decay through H_2O_2 produced during its catalysis.

In this context, we analyzed the production of this enzyme in laboratory mycelial cultures and attacked wood; characterized some molecular, molecular-genetic and catalytic properties of the purified protein; and studied its ultrastructural localization in hyphae and degraded wood. Our findings of the extracellular localization of the enzyme associated with periplasmic and external membranous structures (i.e., tripartite membranes) strongly indicate that *G. trabeum* AOX is a component of the biodegradative system used by this fungus during brown rot decay of wood. The properties of this enzyme are further compared to AOXs from methanol-utilizing yeasts and molds.

MATERIALS AND METHODS

Fungal strain. The brown-rot fungus *G. trabeum* (Persoon: Fries) Karsten strain M617 (ATCC 11539) was obtained from the U.S. Department of Agriculture Forest Products Laboratory (Madison, WI). The fungus was routinely maintained on 2.5% (wt/vol) malt agar plates.

Liquid cultures. The fungus was grown in darkness at 27°C in 500-ml Erlenmeyer flasks containing 80 ml of complex medium (2% glucose, 1.5% corn steep, 0.15% $MgSO_4 \cdot 7H_2O$ in tap water) under reciprocal shaking (8). The medium was adjusted to pH 5.5 with 6 M NaOH before autoclaving. Mildly homogenized cultures derived from malt-agar stock cultures, showing sufficient growth on the same liquid medium, were used for inoculations (6%). Fungal spherical colonies (2- to 8-mm mycelial pellets) for microscopy were harvested 10 and 14 days after inoculation.

Cultures on wood. Four wood blocks (3.0 by 1.5 by 0.5 cm) of birch (*Betula verrucosa* Ehr.) or pine (*Pinus sylvestris* L.) were placed on two pine feeder strips (6.0 by 2.0 by 0.5 cm) previously placed in 500-ml glass bottles (Jena^{ER} Glass) containing garden loam. After autoclaving, the bottles were aseptically inoculated with a mycelial suspension (10 ml) obtained from scraping a single malt agar plate bearing actively growing *G. trabeum* cultures into 100 ml of sterile water and mild homogenization. For the immunofluorescence and transmission electron microscopy (TEM) observations, fungal wood colonization and decay was allowed to proceed at 25°C and 70% humidity for 2 and 4 months. Under these conditions, *G. trabeum* has been shown to produce mass losses of ~30 and 65% in birch and ~20 and 55% in pine wood blocks, respectively.

To assess the possible role of AOX during the fungal attack of pure cellulose, extracted cotton (soaked overnight in benzene-acetone to remove wax) was placed between the wood blocks and feeder strips in some flasks.

Enzyme purification. The enzyme was extracted from washed 14-day-old liquid culture mycelia (13 g [wet weight]) into 75 ml of 50 mM sodium phosphate (pH 7.5) containing 2 mM Pefabloc (Sigma-Aldrich, Prague, Czech Republic) using an Ultra-Turrax (IKA-Werke, Staufen, Germany) homogenizer. Supernatant (crude extract, 77.5 ml) obtained after centrifugation (20,000 × *g*, 20 min) was supplemented with powdered polyethylene glycol 6000 (PEG; Fluka) added slowly under mixing using magnetic stirring to 27% (wt/vol) and then left standing for 30 min at room temperature. The resulting precipitate was pelleted by centrifugation as described above, and the supernatant was discarded. The pellets were extracted into 25 ml of 20 mM sodium phosphate (pH 7.5), and after further centrifugation the supernatant of the extract was directly loaded onto a column (1.5 by 6 cm) of DEAE-Sephacel (Pharmacia Biotech, Uppsala, Sweden) equilibrated with the same buffer. After the column was washed, the bound protein was eluted at 1.5 ml min^{-1} with 250 mM NaCl in the buffer, and 2-ml fractions containing AOX activity were combined (21 ml). Proteins were further fractionated by extensive diafiltration with 20 mM bisTris propane (pH 7.2) (60 ml) on 300-kDa regenerated cellulose ultrafiltration membrane (Millipore, Prague, Czech Republic) with the filtrate discarded and the retentate finally concentrated to 3.6 ml. In the last step, AOX was purified in two portions on MonoQ HR5/5 anion exchanger using a salt gradient from 0 to 350 mM NaCl in 24 ml at a flow rate of 1 ml min^{-1}. Fractions (1 ml) corresponding to the AOX peak maximum at ~130 mM NaCl were combined (2 ml), transferred into 20 mM sodium phosphate (pH 7.5), concentrated, and filter sterilized before storage at 4°C or −80°C.

Enzyme assay. The AOX activity was determined by spectrophotometric measurement (ε_{420} = 42.3 mM^{-1} cm^{-1} [56[) of the production of hydrogen peroxide using a coupled peroxidase reaction with 2,2′azinobis(3-ethylbenzthiazolinesulfonic acid) (ABTS) · $(NH_4)_2$ (Serva, Heidelberg, Germany) as the chromogen. Reaction mixtures (2 ml) at 25°C contained 200 μmol of methanol, 2 μmol of ABTS, 40 μg of horseradish peroxidase (Sigma P-8250), and a suitable amount of AOX in 50 mM air-saturated sodium phosphate (pH 7.5). One unit of AOX was defined as the amount of enzyme activity producing 1 μmol of H_2O_2 (2 μmol of radical cation ABTS) per min under the assay conditions. To assess effect of pH on stability of AOX, the enzyme (0.1 mg ml^{-1}) was kept at 25°C for 1 week at various pH values, and the remaining activity was measured. The following buffers (50 mM) were used: pH 2 to 6, sodium malonate; pH 7 to 9, bisTris propane; and pH 10 to 12, glycine-HCl buffer. The same buffers were used for determining pH optimum of the AOX activity under otherwise standard assay conditions.

Protein concentrations were determined by the bicinchoninic acid method (Sigma procedure TPRO 562) using bovine serum albumin (Sigma) as the standard.

Molecular characterization. The enzyme native molecular mass was assayed by sedimentation equilibrium ultracentrifugation method according to Yphantis (59) by using a Beckman Spinco model E analytical ultracentrifuge equipped with interference optics, rotor AnH-Ti, and 12-mm cuvette (9,341 rpm, 9-h equilibrium, 20°C). The enzyme was dissolved in 50 mM sodium phosphate (pH 7.0) containing 100 mM NaCl. The protein concentration (0.03%) was measured by determining the absorbance at 280 nm. The UV-visible absorption spectra of the purified AOX (2 mg ml^{-1} in 20 mM sodium phosphate [pH 7.5]) were recorded at 25°C on a DU 7400 spectrophotometer (Beckman, Fullerton, CA).

Sodium dodecyl sulfate-polyacrylamide gel electrophoresis (SDS-PAGE) according to the method of Laemmli was carried out on a Hoefer SE 250 apparatus (Amersham, Vienna, Austria) in 10% gels. Analytical isoelectric focusing of the purified enzyme (2 μg) was performed in 1.5% agarose gels (0.5 mm) containing 7.8% Bio-Lyte 3/10 Ampholyte (Bio-Rad, Hercules, CA) by using a Multiphor II system (Amersham) and low-pI standards. Protein bands were stained with Coomassie blue.

For Western analysis, proteins separated by SDS-PAGE were transferred overnight onto nitrocellulose membranes by wet electroblotting (30 V, 90 mA). Membranes were treated with blocking solution containing TBS (10 mM Tris-HCl [pH 7.5], 150 mM NaCl buffer) supplemented with 5% nonfat milk and 0.05% Tween 20 (Sigma). The blots were then incubated with anti-AOX antiserum (1:20,000 in the blocking solution) for 1 h at room temperature. After being washed in TBS (three times for 10 min each time), the membranes were treated with horseradish peroxidase conjugated to donkey anti-rabbit immunoglobulin G (IgG [Amersham]; 1:10,000 in the blocking solution, 45 min). Visualization was carried out with enhanced chemiluminescence (ECL) reagent (Super-Signal West Pico ECL substrate; Pierce, Rockford, IL) on Medical X-ray film (Foma, Hradec Králové, Czech Republic).

Enzyme glycosylation was tested by dansyl hydrazine fluorescence staining for carbohydrate (12) using AOX samples from the final purification step on SDS-PAGE gels. Ovalbumin was used as a positive control.

For N-terminal sequencing, purified AOX was electroblotted onto polyvinylidene difluoride membranes and sequenced by automated Edman degradation on a Procise protein sequencer (Applied Biosystems, Foster City, CA) according to the manufacturer's instructions.

Enzymatic in-gel digestion for mass spectrometry (MS). Coomassie blue-stained protein bands were excised from the SDS-PAGE gel, cut into small pieces, and washed several times with 10 mM dithiothreitol–0.1 M 4-ethylmorpholine acetate (pH 8.1) in aqueous 50% acetonitrile. After complete destaining, the protein was reduced with 30 mM tris[(2-carboxyethyl)phosphine hydrochloride] (TCEP) at 65°C for 30 min and alkylated by treatment with 30 mM iodacetamide (all from Sigma) for 60 min in the dark. The gel pieces were further washed with water, shrunk by dehydration in acetonitrile, and reswelled again in water. The supernatants were removed, and the samples were partly dried in a SpeedVac concentrator. The gel pieces were then rehydrated in a cleavage buffer containing 0.01% 2-mercaptoethanol, 50 mM 4-ethylmorpholine acetate, 10% acetonitrile, 50% of $H_2{}^{18}O$ (Sigma), and 1 μl of protease (50 ng/μl for sequencing-grade trypsin [Promega, Madison, WI] and chymotrypsin; 10 ng/μl for sequencing-grade Asp-N [both from Roche Diagnostics, Mannheim, Germany]). After overnight digestion at 37°C, the resulting peptide mixtures were acidified with 5% acetic acid, and aliquots were purified and concentrated by using C18 ZipTips (Millipore) prior to MS analysis.

MALDI-MS. Positive-ion mass spectra were measured on a Bruker BIFLEX II time-of-flight mass spectrometer (Bruker Daltonics, Bremen, Germany) equipped with a SCOUT 26 sample inlet and a 337-nm nitrogen laser (Laser Science, Cambridge, MA). The spectrum of the intact protein was calibrated externally using $[M+H]^+$ and $[M+2H]^{2+}$ ions of protein standards (trypsinogen,

protein A, and bovine serum albumin [BSA]; Bruker) resulting in the mass accuracy of <0.2%. Sinapinic acid (Bruker) in aqueous 30% acetonitrile–0.1% trifluoroacetic acid (TFA; 10 mg/ml) was used as a matrix-assisted laser desorption ionization (MALDI) matrix. The spectra of the peptides obtained after proteolytic digestion were measured in reflectron mode by using α-cyano-4-hydroxycinnamic acid (Sigma) in aqueous 40% acetonitrile–0.2% TFA (10 mg/ml) as a MALDI matrix. The spectrometer was calibrated externally using the peptide standards angiotensin II and insulin B oxidized form (Bruker) with $[M+H]^+$ ions of 1,046.5 Da and 3,494.6 Da, respectively.

High-pressure liquid chromatography-electrospray ionization MS/MS. Peptide mixtures were loaded onto a homemade capillary column (0.18 by 100 mm) packed with MAGIC C18 (5 μm, 200 Å; Michrom BioResources, Auburn, CA) reversed-phase resin and separated by using a gradient from 5% acetonitrile–0.5% acetic acid to 40% acetonitrile–0.5% acetic acid for 50 min. The column was connected to an LCQ^{DECA} ion trap mass spectrometer (Thermo, San Jose, CA) equipped with a nanoelectrospray ion source. Full scan spectra were recorded in positive mode over the mass range 350 to 2,000 Da. Tandem MS (MS/MS) data were automatically acquired on the three most intense precursor ions in each full scan spectrum and interpreted manually.

MS characterization of prosthetic group. The cofactor was released by heating the protein (4 mg ml^{-1}) at 99°C for 10 min in 25 mM Tris-HCl (pH 8.0). The reaction mixture was filtered by using Microcon YM 10 centrifugal filter device (Millipore), and the ultrafiltrate was analyzed by MALDI-MS using ferulic acid (10 mg/ml in 50% acetonitrile–0.2% TFA; Sigma) as a MALDI matrix. Post-source decay (PSD) fragmentation spectra were recorded in 10 segments, with each succeeding segment representing a 20% reduction in reflector voltage. The segments were pasted, calibrated, and smoothed under computer control by using the Bruker XMASS 5.0 software.

Molecular cloning and sequencing of a cDNA fragment encoding for the AOX protein. Mycelium from *G. trabeum* was harvested from glucose-corn steep medium after 8 to 12 days of cultivation and immediately frozen in liquid nitrogen. Total RNA was isolated from 100-mg (wet-weight) portions of the crushed powder of mycelia by using RNeasy plant minikit (QIAGEN, Valencia, CA) according to the manufacturer's protocol. First-strand cDNA synthesis was done with 5 μg of total RNA with SuperScript III reverse transcriptase (Invitrogen, Carlsbad, CA) and anchored oligonucleotide $d(T)_{23}$ VN primer (NEB). Amplification of the partial cDNA sequence of AOX was done using degenerate forward primer GTRNTE RMFW (5′-ATG GTI CAY CCI GAR GAR GT-3′) derived from N-terminal fragment sequence MVHPEE (see Fig. 3, sequence 1) and the degenerate reverse primer GTRINT1RE (5′-GCI CKI GTR TAC ATY TGR AAR TT-3′) or GTRINT3RE (5′-GYT CIG TIC CRT AIA CRT T-3′) derived from internal peptide fragment sequences NFQMYTRA and NVYGTEH, respectively (Fig. 3, sequences 2 and 3). Alternatively, another forward primer GTRINT4FW (5′-AAR TAY ATG ACI ATG TTY CAR TA-3′) derived from internal peptide fragment KYMTMFQY (Fig. 3, sequence 4) was used in combination with reverse primer GTR3INTRE. All amplifications were done using 35 cycles of PCR with proofreading DNA polymerase *Pfu* Turbo (Stratagene) and a Mastercycler personal cycler (Eppendorf). Three PCR products were obtained with the above primers: a 0.3-kb fragment with the primer pair GTRNTERMFW-GTRINT1RE, a 0.5-kb fragment with the primer pair GTRINT4RE-GTRINT3RE, and a 1.8-kb fragment with the primer pair GTRNTERMFW-GTRINT3RE. All PCR products were cloned into pBluescript SK(+) vector (Stratagene) and further propagated in *Escherichia coli*. Plasmid DNA was prepared, and the cloned inserts were sequenced by using automated DNA sequencer (ABI Prism 3100) according to the manufacturer's protocols.

To confirm the sequence of 5′ cDNA end and obtain the missing 3′-end sequence, a BD SMART RACE cDNA amplification kit (Clontech) was used. Two cDNA templates were produced using 1 μg of total RNA for 5′-RACE and 3′-RACE reactions, respectively. 5′-RACE and 3′-RACE amplifications were performed using 30 cycles of PCR with BD Advantage 2 DNA polymerase (Clontech). A common universal primer (UPM) was used for the amplifications of cDNA ends together with two distinct gene-specific primers: 5′-RACE reverse primer (5′-TTC ATA AAG CCC GAG TCG AAG AAG-3′), and 3′-RACE forward primer (5′-GGC ACA CGG GCA GGC GCA GCG ACG CC-3′). The resulting PCR products (a 1.4-kb 5′-RACE PCR product and a 1.5-kb 3′-RACE PCR product) were cloned and sequenced as described above. The sequence data obtained from all of the individual PCR fragments were combined to provide a complete sequence of *AOX* gene.

Polyclonal antibody. Polyclonal antibody production against purified AOX was carried out in New Zealand White rabbits by subcutaneous injections of the highly purified protein (2.5 mg) dissolved in 1 ml of Freund complete adjuvant (Difco Laboratories, Detroit, MI) and 0.2 ml of 9% NaCl as previously described (8).

Sample preparation for fluorescence microscopy. All samples were fixed in 4% (vol/vol) paraformaldehyde in 0.1 M phosphate-buffered saline (PBS; pH 7.2) containing Tween 20 (0.001%) for 2 h at room temperature, followed by three rinses in PBS (15 min each under agitation). *G. trabeum* colonies (small pellets) from liquid cultures were then embedded in Paraplast (Sigma) and sectioned on a motorized microtome (HM 350; Microm, Germany). Semithin sections (6 to 8 μm) were placed on poly-L-lysine-coated slides and used for immunocytochemistry after Paraplast removal by xylene, followed by rehydration (4). Wood samples were sectioned (20 μm) on a Leica microtome (Leica Microsystems, Wetzlar, Germany) equipped with Feather disposable blades and used directly for immunofluorescence observations without embedding.

Immunofluorescence labeling of alcohol oxidase. For AOX-antibody labeling of fixed hyphae in sections and whole mycelium mounts from liquid cultures, wood sections from degraded wood blocks, and cotton fibers, specimens were first treated by 30 min of blocking in PBS containing 10% (wt/vol) glycine. Samples were washed in PBS (10 min each) and blocked again for 1 h in normal goat serum (Sigma) in PBS containing 1% BSA (1:3). Samples were then washed (three times for 10 min each time) and incubated overnight at 4°C in AOX antiserum diluted 1:200 or 1:500 in PBS supplemented with 1% (wt/vol) BSA. Thereafter, samples were washed three times in distilled water (for 30 min each time) on a rotary shaker, followed by incubation in goat anti-rabbit-fluorescein isothiocyanate (FITC)-conjugated IgG (Sigma) diluted 1:500 in 10 mM Tris-HCl buffer (pH 7.2) containing 1% (wt/vol) BSA for 1 h in the dark. After three final washes in Tris-HCl buffer (pH 7.2), the samples were counterstained using 1 μg of DAPI (4′,6′-diamidino-2-phenylindole; Roche Diagnostics, Mannheim, Germany)/ml for visualization of the fungal nuclei. The following labeling controls were included: (i) substitution of the AOX antiserum with PBS-BSA; (ii) AOX antisera preabsorbed with freshly prepared AOX protein (1:10 protein equivalents); (iii) treatment of samples with anti-phospho-insulin receptor/insulin-like growth factor 1 receptor (Sigma I2033) as an irrelevant antisera; and (iv) labeling of sections derived from birch and pine wood colonized by the mold fungi *Aspergillus niger* (CBS 246.15) or *Penicillium citrinum* (CBS 342.61). In addition, hyphae from whole-mount pellets from 4-day-old liquid cultures (before AOX induction, see Fig. 1) were labeled with AOX antisera.

All of these steps except for the primary antibody treatments were carried out at room temperature. Labeled and control samples (sections or whole-mycelium mounts) were placed on object glasses, mounted in Fluorsave (Calbiochem/Merck, Darmstadt, Germany), covered by coverslips, and examined by fluorescence microscopy (Leica) using a standard set of filters for FITC, TRITC (tetramethyl rhodamine isothiocyanate) (rhodamine), and DAPI. Images were recorded with a charge-coupled device camera (Leica DC 300F) using a digital imaging system for professional microscopy (Leica) with one exposure time (3.5 s) for all samples.

Sample preparation for TEM. For TEM, small spherical *G. trabeum* mycelium colonies removed from 10- and 14-day-old agitated liquid cultures or small wood slivers removed from degraded wood blocks (2 or 4 months) by using a razor blade were fixed for 3 h in 3% (vol/vol) glutaraldehyde containing 2% (vol/vol) paraformaldehyde in 0.1 M sodium cacodylate buffer (pH 7.2) at room temperature. Samples were then washed three times in the buffer (for 15 min each time) and postfixed in 1% (wt/vol) osmium tetroxide in 0.1 M buffer for 1 h at room temperature. After further washes in the buffer and distilled water, the samples were dehydrated in an ethanol series (20 to 100% ethanol; 10% steps, 10 min each time), infiltrated with London resin (London Resin Co., Basingstoke, United Kingdom), and polymerized overnight at 60°C. Additional samples were fixed for 3 h in 4% (vol/vol) paraformaldehyde containing 0.1% (vol/vol) glutaraldehyde in the same buffer and thereafter dehydrated and infiltrated with resin as described above. Ultrathin sections of selected material were cut (primarily transverse sections) by using a Reichert FC4 ultramicrotome, and sections were collected on nickel grids stained with ethanolic (50%) 4% (wt/vol) uranyl acetate. Observations were made using a Philips CM12 transmission electron microscope operated at 60 or 80 kV.

TEM-immunocytochemistry studies. Ultrathin sections for immunolabeling were processed as described previously (7). Nickel grids bearing sections were incubated in anti-AOX (1:100 or 1:500) in PBS (pH 7.4) containing 1% (wt/vol) BSA and 0.05% (vol/vol) Tween 20 and left overnight at 4°C. After primary AOX incubation, sections were washed in PBS-BSA-Tween 20, followed by Tris-HCl–BSA–Tween 20 (pH 8.4), and subsequently gold labeled with goat anti-rabbit immunoglobulin G conjugated to 15-nm-diameter Au probes (Janssen Life Science Products, Beerse, Belgium). Poststaining was performed as described above. Controls included the omission of the AOX primary or secondary antibody labeling stages.

Nucleotide sequence accession number. The GenBank/EMBL/DDBJ database accession number for the *G. trabeum AOX* gene in the present study is DQ835989 (http://www.ncbi.nlm.nih.gov).

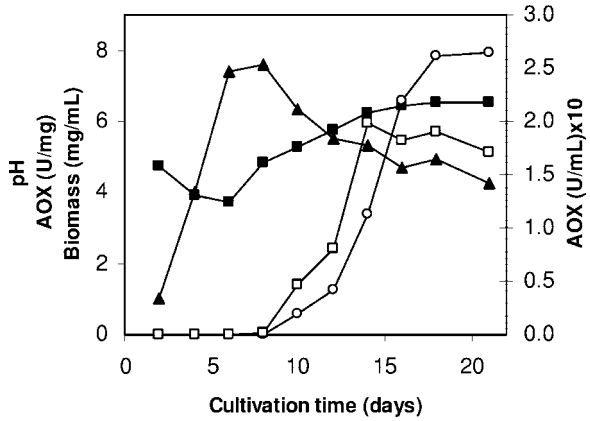

FIG. 1. *G. trabeum* growth curve on 2% glucose–corn steep medium and time profiles for AOX. Enzyme activity was assayed with methanol as the substrate by measuring H_2O_2 production through a coupled reaction with peroxidase and chromogen. Symbols: ▲, growth (mg of mycelial dry weight ml^{-1}); □, production of AOX (U per mycelial mass in 1 ml of culture); ○, AOX specific activity (U mg of $protein^{-1}$; ■, pH of the culture liquid. All data points were obtained for samples taken from quadruplicate cultures harvested and combined at the same time.

RESULTS

AOX production and purification. Figure 1 shows the typical growth pattern of *G. trabeum* in submerged liquid cultures and AOX production. Synthesis of this enzyme was induced in the stationary growth phase after ~9 days of cultivation when the pH, after an initial decline, began rising above its original value of pH 4.8. AOX was isolated from extracts of mycelia harvested from the 14-day-old submerged cultures, when AOX activity had reached its maximum of ~0.2 U ml of $culture^{-1}$ and represented a major protein band in the protein pattern expressed by the fungus (Fig. 2, lane 4).

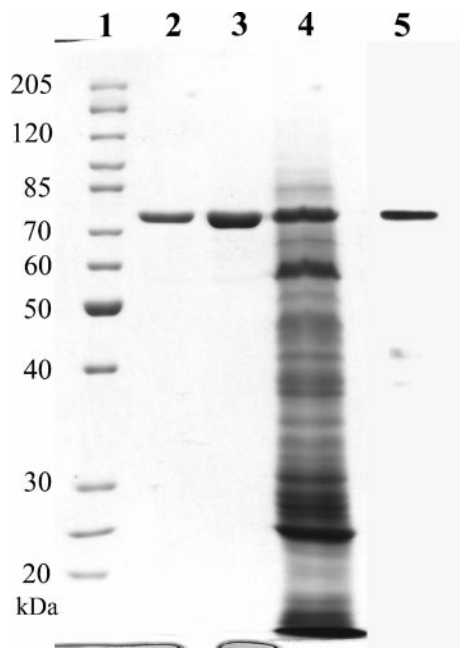

FIG. 2. SDS-PAGE and Western analysis of AOX purified from *G. trabeum*. Lane 1, standard molecular weight protein ladder (Fermentas, Vilnius, Lithuania); lanes 2 and 3, AOX from the final purification step on MonoQ; lane 4, sample of the crude mycelium extract; lane 5, Western blot of mycelium extract (16 μg of total protein per well) showing a single protein band of AOX after ECL-immunostaining with polyclonal anti-AOX antibodies (see Materials and Methods).

TABLE 1. Purification of AOX from *G. trabeum*[a]

Purification step	Total protein (mg)	Total activity (U)	Sp act (U mg^{-1})	Recovery (%)	Purification (fold)
Crude extract	58	81	1.4	100	1
PEG precipitation	40	73	1.8	90	1.3
DEAE Sephacel	13	71	5.5	88	3.9
300-kDa UF	8.2	69	8.4	85	6.0
MonoQ	3.3	41	12	51	8.6

[a] The initial total protein was measured by using the Bradford method. Protein in samples of (partially) purified AOX was determined using the bicinchoninic assay. For the AOX activity assay, see Materials and Methods.

Results from a representative AOX purification procedure are summarized in Table 1. The enzyme was purified 8.6-fold from the crude mycelial extract with an overall yield of ~51% and a specific activity of 12 U mg of $protein^{-1}$ under standard assay conditions. The highly purified protein gave a single band on SDS-PAGE (Fig. 2, lanes 2 and 3). One-week storage of the sterile-filtered purified enzyme in 20 mM sodium phosphate (pH 7.5) at 4°C resulted in a 68% loss of activity. The activity was then relatively stable for an additional 2 weeks (≤3% loss of activity). Rapid freezing at −80°C and thawing had no significant effect on the enzyme's activity.

Molecular properties. The AOX's native molecular mass of 628 ± 19 kDa was calculated from equilibrium ultracentrifugation data, assuming a partial specific volume of 0.75 $cm^3\ g^{-1}$, which compares well with the value of 610 ± 5 kDa estimated for *Poria contigua* AOX using the same partial specific volume (3). SDS-PAGE gave a band at 73 kDa (Fig. 2) in agreement with the subunit molecular mass determined by MALDI-MS of 72.4 kDa, suggesting that the enzyme is an octamer. Analytical isoelectric focusing of the purified protein confirmed its apparent homogeneity and gave an isoelectric point of 5.3.

Solutions of purified AOX (2 mg of protein ml^{-1} in 20 mM sodium phosphate [pH 7.5]) had a brownish color and exhibited a UV-visible absorption spectrum with maxima at 280, 390, 404, and 458 nm and a shoulder at 477 nm. The A_{390}/A_{404} maximum ratio was concentration dependent, increasing its value with the enzyme dilution. The A_{280}/A_{458} ratio was 15.7. Treatment of purified AOX with 5% trichloroacetic acid, followed by heating, released the flavin moiety from the holoenzyme, suggesting its noncovalent attachment to the polypeptide. The cofactor was also released by heating the protein for 10 min in 25 mM Tris-HCl. MALDI-MS analysis of the released cofactor in the ultrafiltrate of the latter reaction mixture gave an intense peak at *m/z* 786 corresponding to $[M+H]^+$ ion of unmodified flavin adenine dinucleotide (FAD). The presence of standard FAD was further confirmed by fragmentation using PSD analysis. The PSD spectrum was dominated by peaks of complementary ions *m/z* 348 (AMP fragment) and *m/z* 439 consisting of ribitol and isoalloxazine ring. The ions

TABLE 2. Substrate specificity of AOX from *G. trabeum* with respect to electron donors (100 mM)[a]

Substrate	Relative activity (%)	k_{cat}/K_m (s^{-1} mM^{-1})
Methanol	100	6.8
Ethanol	94	1.1
Allyl alcohol	93	0.53
1-Propanol	73	0.26
1-Butanol	54	0.07
1-Pentanol	22	0.03
2-Methyl-1-propanol	7	
3-Methyl-1-butanol	7	
2-Propanol	5	
tert-Butanol	<4	
(±)-2-Butanol	<4	
3-Pentanol	<4	
2-Butene-1,4-diol	4	
Benzyl alcohol	9	
4-Hydroxybenzyl alcohol	<4	
D-Arabinitol	6	
D-Glucose	8	
Ethanolamine	<4	

[a] Activities are given relative to methanol. Catalytic efficiency constants (k_{cat}/K_m) are given for the six major substrates.

m/*z* 250 and 136 comprising ribose plus adenine and adenine alone were also observed (data not shown).

G. trabeum AOX is apparently not a glycoprotein, as was demonstrated by negative staining using the dansyl hydrazine method (data not shown). This is supported by good agreement of experimental (72.4 ± 0.14 kDa) and theoretical molecular mass based on the primary structure of the mature protein (72.382 kDa). Similar negative findings were reported for *Polyporus obtusus* and *Peniophora gigantea* AOX analyzed for carbohydrate content by the anthrone method (29) and concanavalin A precipitation test (11), respectively.

Catalytic properties. The purified *G. trabeum* AOX exhibited a broad substrate tolerance toward oxidation of short-chain primary alcohols (Table 2). Some polyols were also significantly oxidized, whereas secondary alcohols and aryl alcohols were very poor substrates. The apparent kinetic constants determined for methanol under air-saturated (~0.23 mM O_2 at 25°C [57]) conditions were K_m = 2.3 mM, V_{max} = 12.9 μmol of H_2O_2 min^{-1} mg of $protein^{-1}$, k_{cat} = 15.6 s^{-1}, and k_{cat}/K_m = 6.8 s^{-1} mM^{-1}. Comparison of the catalytic efficiencies (k_{cat}/K_m) for five major AOX substrates (Table 2) indicates that methanol is clearly the preferred AOX substrate.

AOX had a pH stability optimum on the alkaline side in the range of pH 7 to 11 (>80% maximum stability at pH 9). A broad optimum pH range with activity almost constant at pH 6 to 10 (>96% maximum activity at pH 6.5) was followed by a rapid decrease of activity on both alkaline and acidic side, with 16% of activity left at pH 5.5 and no activity detectable at pH 5.0 and 12. The decrease on the acidic side is clearly due to the high instability of the enzyme at pHs of ≤5.5 and not due to the coupled peroxidase assay used with horseradish peroxidase activity optimum at pH 6 (BRENDA database).

AOX primary sequence. With PCR primers based on the available N terminus of the purified mature protein and internal peptide sequences determined by high-pressure liquid chromatography-electrospray ionization MS/MS (Fig. 3), *AOX* cDNA fragments were obtained from *G. trabeum* mRNA by reverse transcription-PCR using degenerate primers as described above, and the missing 5′ and 3′ ends of the cDNA were characterized by means of the RACE method (see Materials and Methods). The complete cDNA sequence compiled from independent overlapping sequence fragments codes for 651 amino acids (Fig. 3).

As evidenced by Edman degradation and MS sequencing data (Fig. 3), the initiator methionine was removed cotransla-

```
                1
MVHPEEVDVI VCGGGPAGCV VAGRLAYADP NLKVMLIEGG ANNRDDPWVY RPGIYVRNMQ RDGVNDKATF    70
                                          2
YTDTMKSSHL RGRQAIVPCA NILGGGSSIN FQMYTRASAS DWDDFKTEGW TCQDLLPLMK RLENYQKPVN   140
***
NDTHGYDGPI AISNGGQITP LAQDFLRAAH SIGVPYSDDI QDLTTAHGAE IWAKYINRHT GRRSDAATAY   210
VHSVMDVQTN LYLRTNARVS RVIFEGNKAV GVAYVPSRNR AHGGAVLETI VKARKCVVLS SGTLGTPQIL   280
                                      ***
ERSGVGNGEL LKKLDIKVVS DLPGVGEQYQ DHYTTLSIYR VSNDSITTDD FLRGVKEVQR ELFQEWETSP   350
                                                                    4
EKARLSSNVI DAGWKLRPTE EELKEMGPEF NELWDRYFKD KPDKPVMFGS IVAGAYADHT LLPPGKYMTM   420
FQYLEYPASR GKIHIQSTNP YKEPFFDSGF MNNKADFAPI RWSYKKTREV ARRMDAFRGE LTSHHPHFHP   490
ASAAATRDID IKTAKEIYPD GLTVGIHMGT WHRPSEPFDA SKVHEDIKYT EEDDKAIDDW VADHVETTWH   560
                        3
SLGTCAMKPR EQGGVVDKRL NVYGTEHLKC VDLSICPDNL GTNTYSSALL VGEKGADLLC EELGLKVRVP   630
HAPVPHAPVP TGRPATQQPK H                                                       651
```

FIG. 3. Amino acid sequence of *G. trabeum* AOX derived from cDNA. The sequence stretches used for the construction of degenerate PCR primers are numbered (see Materials and Methods). Sequence confirmation using both peptide mass mapping and tandem mass spectrometry (boldface), peptide mass mapping only (underlined), and automated Edman degradation (double underlined) is labeled. In the mature protein, the initiator methionine is removed from the N terminus by methionine aminopeptidase. Potential sites of N glycosylation are marked with asterisks.

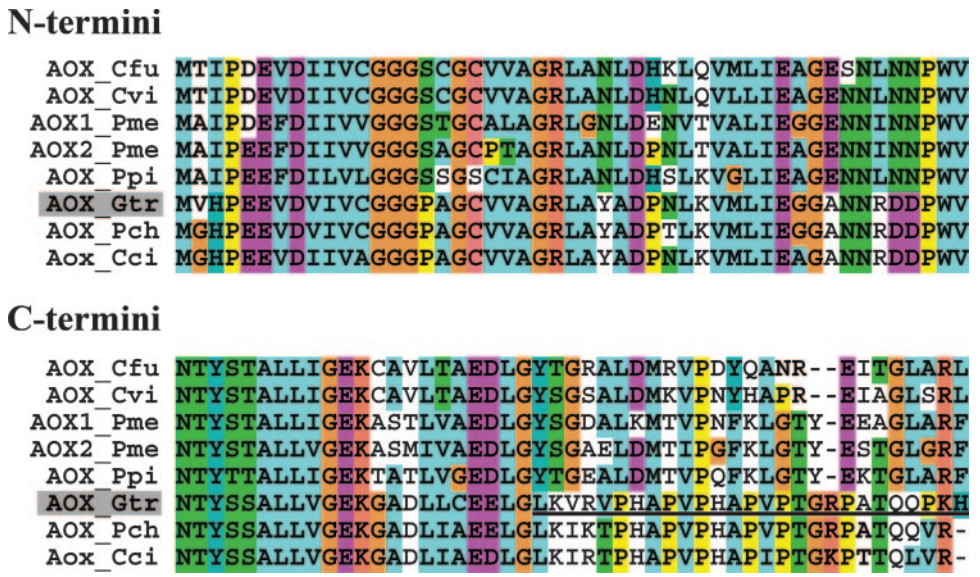

FIG. 4. Multiple sequence alignment of N and C termini of *G. trabeum* (Gtr) AOX with the termini of yeast and mold AOXs. Known AOXs: Pme, *Pichia methanolica*; Ppi, *P. pinus*; Cvi, *Cochliobolus victoriae*; Cfu, *Cladosporium fulvum*. Two predicted AOXs: Pch, *Phanerochaete chrysosporium*; Cci, *Coprinus cinereus*. The unique sequence of the last 27 C-terminal amino acids of *G. trabeum* AOX is underlined.

tionally by the action of methionine aminopeptidase, and it was not present in the isolated mature protein. Furthermore, no cleavage of signal peptide from the N terminus during protein posttranslation processing and translocation was observed. The putative C-terminal peroxisome targeting signal 1 (PTS1) of methylotropic yeast/mold AOXs interacting with the Pex5p receptor protein to direct reporter proteins into the peroxisomal matrix (55) was missing (Fig. 4).

Immunofluorescence and immunogold-TEM of AOX in *G. trabeum* hyphae grown in liquid cultures. Using fluorescence

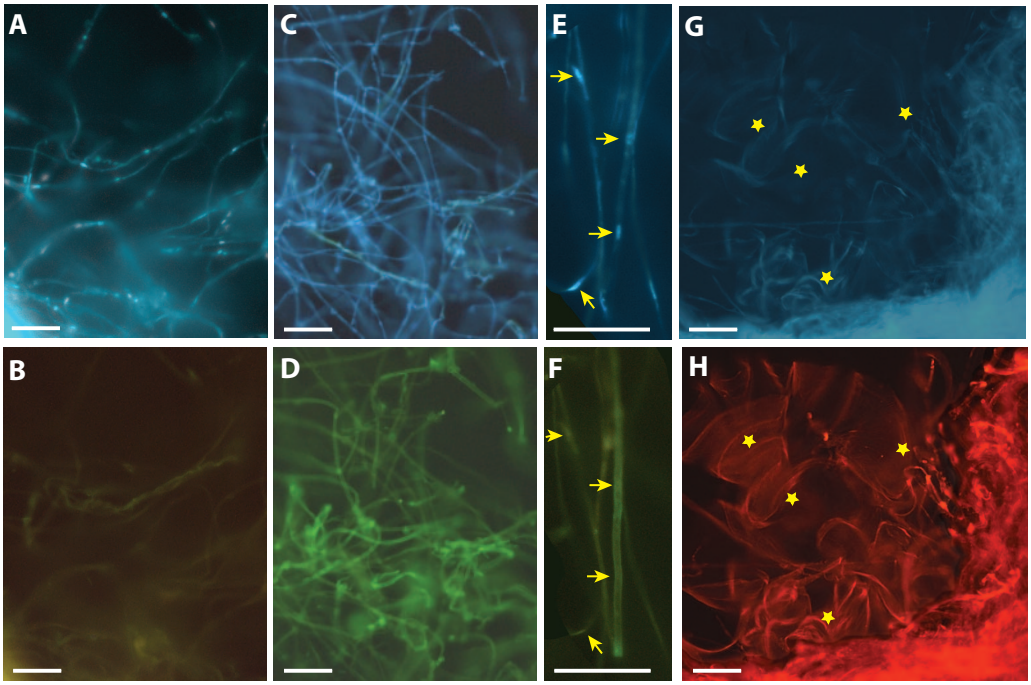

FIG. 5. AOX immunofluorescent localization on whole mycelia and hyphae from 10- and 14-day-old liquid cultures of *G. trabeum*. (A and B) Control double labeling of 10-day-old culture by DAPI (A) and anti-rabbit IgG-FITC (B); (C and D) double labeling of 10-day-old culture by DAPI (C) and anti-AOX-IgG-FITC (D). All hyphae were strongly labeled by AOX. (E and F) Double labeling of 10-day-old culture by DAPI (E) and anti-AOX-IgG-FITC (F). The signal for AOX was strong on the hyphal wall (yellow arrows) often in regions where DAPI showed a strong signal for nuclei. (G and H) Double labeling of 14-day-old culture using DAPI (G) and anti-AOX-IgG-TRITC (H). Extracellular slime materials (stars) within the *G. trabeum* pellets showed a strong reaction with the AOX antibody. Bars, 50.0 μm.

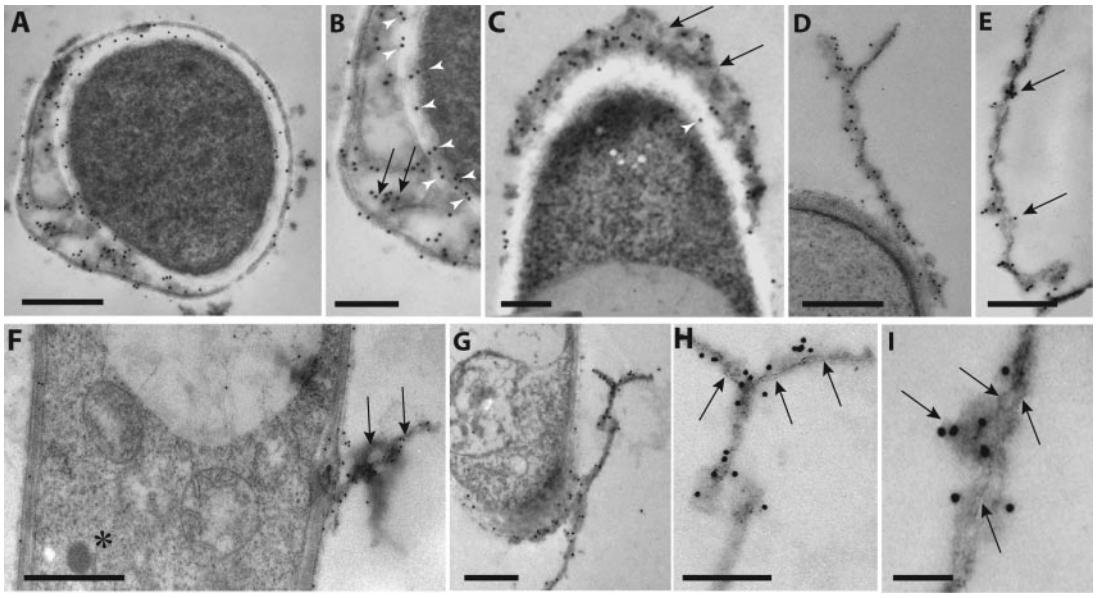

FIG. 6. AOX TEM-immunogold labeling of hyphae from 14-day-old agitated liquid cultures of *G. trabeum*. (A to C) Transverse sections of hyphae showing strong labeling of the hyphal cell wall (arrowhead in panel B), intrahyphal materials (arrows in panel B), and periplasmic space and electron-dense extracellular slime materials associated with the outer hyphal wall (arrows in panel C). (D to G) Strong AOX labeling of extracellular tripartite membrane structures emanating from the outer hyphal cell wall. (E, H, and I) High magnification images showing the extracellular tripartite membrane structure with AOX mostly associated with the electron dense materials coating the membranes (arrows). (F) Longitudinal section through a hypha showing strong positive AOX labeling of extracellular materials on tripartite membranes (arrows, right side) and negative labeling of a cytoplasmic peroxisome (asterisk, left side). Bars: A, D, E, F, and G, 0.5 μm; B, C, and H, 0.25 μm; I, 0.1 μm.

microscopy (AOX-FITC or AOX-TRITC labeling), *G. trabeum* hyphae from liquid cultures (10 and 14 days) labeled strongly for the presence of AOX (Fig. 5). AOX was located along the fungal cell wall and associated with extracellular slime materials coating hyphae and present within the main slime matrix of the mycelial pellets (ca. 2 to 3 mm in width) produced during culturing (Fig. 5C to H). The enzyme was associated with both active (i.e., indicated by presence of positive staining nuclei with DAPI) and necrotic hyphae lacking nuclei (Fig. 5C to F). Strong AOX labeling was noted on the cut ends (i.e., through sectioning) of hyphae within pellets, as well as small localized zones on the hyphal surface (Fig. 5D and F, arrows). Little difference in labeling was noted between the 10- and 14-day-old cultures, although the mycelia from the latter cultures showed a stronger labeling and a positive response of all mycelia and associated slime materials.

TEM-immunogold labeling of sectioned hyphae from 14-day-old cultures showed strong labeling of intrahyphal cell wall regions (Fig. 6A and B), periplasmic space, hyphal walls, and extracellular slime materials adhering to the outer walls of hyphae (Fig. 6A to G). Within the intrahyphal wall region, AOX labeling was localized on more darkly staining structures reminiscent of the outer cell wall materials (Fig. 6B, arrows). In particular, strong AOX labeling was present on extracellular structures released from the hyphal walls of *G. trabeum* (Fig. 6C to G). These structures were membranous being composed of double or tripartite-like membrane structures (Fig. 6H and I). Labeling was mostly associated with the more intensely staining materials adhering to both sides of the membrane structures (Fig. 6H and I). At high magnifications, slime material associated with the outer hyphal wall also had an oriented structure containing membranous structures (Fig. 6C, arrows). Sectioned hyphae occasionally showed intracellular darkly staining microbodies presumed to be peroxisomes (Fig. 6F, asterisk). Although these structures remained unlabeled, extracellular materials from the same hyphal regions showed strong labeling for AOX (Fig. 6F, arrows). Occasional labeling of intracellular endoplasmic reticulum was also noted. The results from both 10 days and 14 days were similar in the spatial distributions of AOX, the longer time period producing more-intense labeling.

All control labelings, including (i) omission of the AOX primary antibody labeling stage, (ii) use of preabsorbed AOX, and (iii) use of inappropriate antisera with liquid culture hyphae and wood sections, gave negative results for immunofluorescence (Fig. 5A and B) and immunogold labeling (not shown). Hyphae from mold-colonized wood were also negative for AOX. Some hyphae from pellets of 4-day-old liquid cultures showed weak labeling, suggesting that either hyphae were remaining from the initial inoculating cultures or induction of AOX may be slightly earlier than that indicated by the spectrophotometric enzymatic assay.

Immunofluorescence and immunogold-TEM analyses of AOX in *G. trabeum* hyphae grown on wood and cotton. Immunofluorescence labeling of wood sections from birch and pine was carried out after degradation for various time periods ranging from 2 to 4 months, i.e., at a time when decay and mass loss for wood blocks lies in the region of ca. 30 to 65% for birch and ca. 20 to 55% for pine. Labeling of both transverse radial and tangential longitudinal sections was carried out, and most fluorescence labeling was done with anti-AOX, followed by IgG conjugated to FITC rather than TRITC because of the

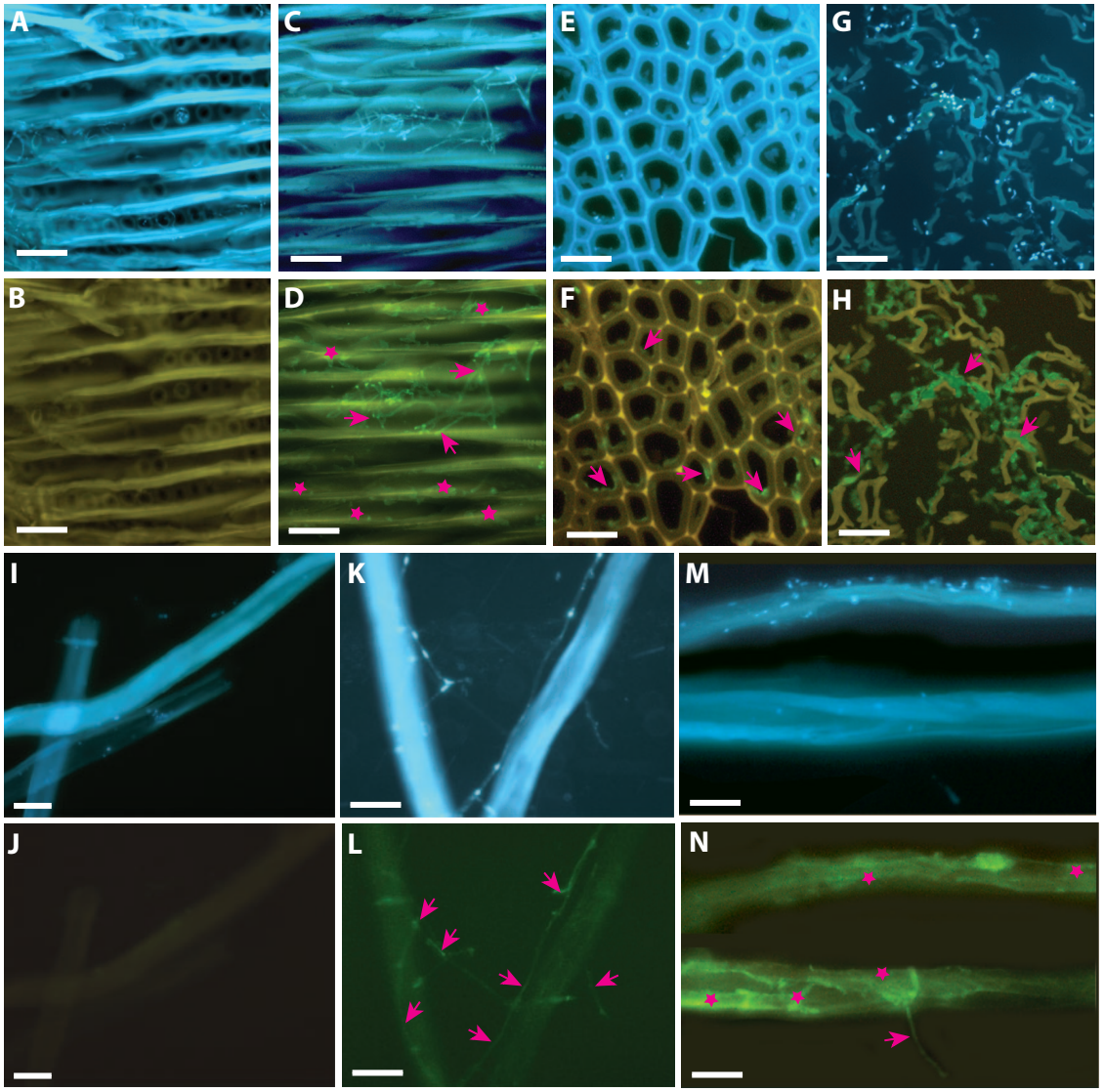

FIG. 7. AOX immunofluorescence localization of *G. trabeum*-attacked birch and pine wood and cotton fibers. (A and B) Control double labeling of pine wood (3 weeks of decay) with DAPI (A) and rabbit-IgG-FITC (B) showing yellow background typical for autofluorescence of lignin (radial longitudinal sections [RLS]). (C and D) Double labeling of pine wood (3 weeks of decay) with DAPI (C) and anti-AOX-IgG-FITC (D). *G. trabeum* hyphae are strongly labeled (arrows), as are extracellular materials (stars) distant to the hyphae associated with the wood cell walls (RLS). (E and F) Double staining of transverse sections of birch wood (3 weeks decay) with DAPI (E) and anti-AOX-IgG-FITC (F). *G. trabeum* hyphae and extracellular materials associated within the cell lumen surface label strongly for anti-AOX-IgG-FITC (pink arrows), as do hyphae located within the fiber secondary cell walls. (G and H) Double labeling of transverse sections of pine wood (2 months of decay) with DAPI (G) and anti-AOX-IgG-FITC (H). The wood sample is highly degraded and has fallen apart during sectioning. *G. trabeum* hyphae and extracellular materials are strongly AOX positive, giving an intense green signal (pink arrows). (I and J) Control double labeling of cotton fibers (2 weeks of decay) with DAPI and rabbit-IgG-FITC. Minimal background fluorescence was noted. (K, M, L, and N) Double labeling of cotton fibers (2 weeks of decay) with DAPI (K and M) and anti-AOX-IgG-FITC (L and N). Active *G. trabeum* hyphae (DAPI labeling) show strong labeling for AOX on hyphae (pink arrows) and extracellular materials (stars). Bars: A to K and M, 100 μm; L to N, 50.0 μm.

better differentiation of the wood cell walls (i.e., they appear yellowy with FITC because of the autofluorescence of lignin; Fig. 7B) and *G. trabeum* hyphae. Observations on fresh sections showed strong labeling of green hyphae within the cell lumina of both the birch and the pine samples studied, showing the presence of AOX (Fig. 7C to H). Hyphae were often distinct against the lumen wall, and the presence of extracellular AOX was demonstrated by green fluorescence of localized neighboring wood fiber cell wall regions (Fig. 7C to H). This was not apparent in control samples (Fig. 7A and B). Fluorescence labeling was also carried out on colonized and degraded cotton fibers sandwiched between wood blocks and incubated for periods of 2 weeks to 2 months. Cotton fibers removed after 2 months of colonization by *G. trabeum* showed hyphae directly attached and associated with the degraded cotton fibers to be positively labeled for AOX similar to the hyphae from the liquid cultures and those colonizing wood blocks (Fig. 7K to N).

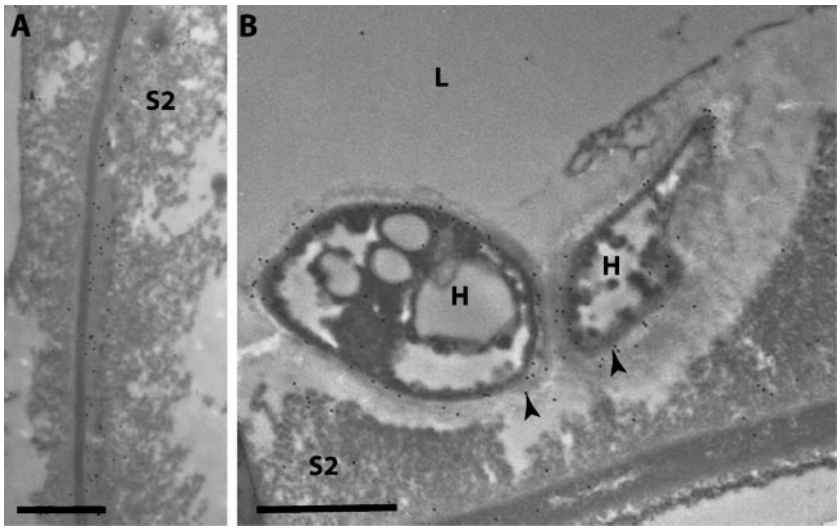

FIG. 8. AOX immunogold labeling of *G. trabeum* 4-month-old highly degraded birch wood. (A) Highly degraded fiber wall region remote from hyphae showing the very open structure of the S2 layer (mostly lignin remaining) and positive labeling for extracellular AOX. (B) Transverse section showing positive AOX labeling of hyphae growing within the secondary cell wall (S2 layer) of a fiber. Both the hyphal cell wall and the extracellular slime materials are AOX positive (arrowheads). The fiber is almost totally degraded, and only a lignin skeleton remains. Note that fiber wall materials partially surrounding and lying beneath the hyphae, including lignin, appear degraded. L, fiber lumen; S2, secondary cell wall layer. Bars: A, 0.10 μm; B, 0.25 μm.

Decay of wood by *G. trabeum* is thought to occur by attack and dissolution of the surrounding wall celluloses and hemicelluloses by hyphae localized in the cell lumina. In the present study we also found *G. trabeum* hyphae to be not only associated with the luminal surface of fibers and parenchymatous cells but also present within the actual secondary S2 wall layer (i.e., the dominating wood cell wall layer) as well as "sunken" into the S2 wall from the lumen (Fig. 8A). Details concerning the ultrastructural aspects of cell wall decay by *G. trabeum* will be published elsewhere. Figure 8 shows typical AOX labeling of hyphae associated with highly degraded birch fibers in transverse sections. The fiber wall shows advanced decay, and the S2 cell wall has a very open structure consistent with the removal of much of the cellulose and hemicellulose components. Positive AOX labeling was found on the hyphal cell walls and associated extracellular materials, both situated within the fiber S2 wall layer (Fig. 8B); results consistent with the immunofluorescence observations (Fig. 7F). Evidence for the presence of AOX was also found in highly degraded wood cell wall regions remote from hyphae (Fig. 8). Control labeling of degraded wood and cotton fibers (i.e., omission of the antibody stage) were all negative (not shown).

DISCUSSION

Enzyme properties. Production of AOX in laboratory cultures of *G. trabeum* was reported as early as 1969 (34), but the enzyme has not been characterized previously. The enzyme we purified from this brown rot fungus shares most of the basic biochemical characteristics of AOXs (alcohol:oxygen oxidoreductase EC 1.1.3.13) reported previously for a number of yeasts and filamentous fungi (44). Like other enzymes of the glucose-methanol-choline oxidoreductase family, it is an inducible nonglycosylated homooctameric O_2-dependent FAD flavoprotein oxidizing short-chain primary aliphatic alcohols into the corresponding aldehydes with concomitant production of H_2O_2. Methanol is the preferred substrate, as found for methylotropic yeast AOXs, as well as the AOXs thus far partially characterized from the basidiomycete fungi *Poria contigua* (3), *Peniophora gigantea* (11), *P. obtusus* (29), and *Phanerochaete chrysosporium* (14). It is well documented that during wood deterioration by these fungi, methanol is produced upon enzymatic demethylation of lignin substructures (1, 16). Interestingly, relatively high activity of AOX toward allyl alcohol may also be related to lignin substructures (based on methoxy[hydroxyphenyl]allyl alcohol), specifically allyl alcohol side groups exposed after initial lignin demethylation and partial depolymerization.

G. trabeum AOX seems to be strictly bound to the demonstrated extraneous membrane structures and polysaccharide hyphal sheath because we could not detect significant activities in culture filtrates. This may also be due to the instability of the enzyme at pHs of <7, which is the case of the laboratory liquid cultures under study. However, its activity was readily released on applying the relatively mild extraction procedure at pH 7.5 using Ultra-Turrax homogenization (see Materials and Methods). Unlike the AOX from *P. gigantea* that displayed a covalently bound FAD (11), the FAD cofactor of *G. trabeum* AOX was easily dissociated by heat treatment similar to that thus far characterized for yeast AOXs (44).

Sequence analysis and alignments. Genes encoding AOX have thus far been identified, and cDNAs have been cloned from several yeasts (38, 44, 51) and mold fungi (27, 44, 48, 49). Here we present for the first time the primary structure of AOX from a basidiomycete fungus that compared to the yeast and/or mold enzymes exhibited some unique features.

The deduced amino acid sequence displayed 51 to 53% identity and 67 to 70% similarity to other AOX sequences when comparisons were made with the known protein se-

quences in GenBank using the BLAST algorithm (for the organisms, see the legend to Fig. 4). Sequence identity percentages for alignments of yeast-yeast and mold-yeast AOXs were, in contrast, significantly higher (72 to 99% and 65 to 70%, respectively), indicating a certain developmental divergence. This is consistent with the earlier-reported immunological incompatibility of AOX from *Poria placenta* with yeasts AOX and the deduced differences in protein primary structures (3).

Based on genome database searches, predicted sequences for AOX were also obtained for two other basidiomycete fungi: *Phanerochaete chrysosporium* (JGI Eukaryotic Genomics project; http://genome.jgi-psf.org) and *Coprinus cinereus* (Southeast Fungal Biology Group; http://genome.semo.edu). Their comparison with the *G. trabeum* AOX interestingly showed much higher sequence identities of 88 and 85%, respectively, against the above yeast and mold sequences.

In general, N termini of the known AOXs show high similarities (Fig. 4), whereas the sequence for the last 27 C-terminal amino acids of *G. trabeum*'s AOX is characteristic of this enzyme and homologous only to the C termini of the predicted AOXs from the related lignocellulolytic basidiomycete fungi discussed above (Fig. 4), suggesting a similar role for the enzyme. Unlike the corresponding carboxy-terminal sequences of yeast and mold AOXs, the C termini of the three basidiomycete AOXs do not contain the PTS1 LARF-(like) tetrapeptide shown previously to direct reporter proteins to peroxisomes (55). Absence of this motif is consistent with our findings of the extracellular localization of *G. trabeum* AOX using immunofluorescence and TEM labeling. Deletion of the C-terminal PTS1 in the mutant yeast *AOX* gene had, however, no (23) or limited (55) effect on protein sorting, which suggested that the yeast AOX contains another, internal PTS recognized by HpPex5p (PTS1 receptor). The proposed novel HpPex5p-dependent AOX import pathway does not require PTS1 and the C-terminal TRP motif of HpPex5p. Instead, only the N-terminal part of HpPex5p and a thus-far-unidentified internal PTS (putative PTS3) activated upon FAD binding are essential to mediate AOX translocation (23). This was, among others, shown by mislocalization to the cytosol of *Hansenula polymorpha* AOX mutated in the dinucleotide binding fold. Signaling adaptation that has changed the interaction of the yeast AOX with Pex5p into the above novel mode of binding dependence on FAD-internal PTS3 is thought developed as a physiological advantage specifically by methylotropic yeasts (23). Similarly, from an evolutional point of view, a proper developmental modification at the C-terminal PTS1 motif of *G. trabeum* AOX may thus divert its targeting from peroxisomes to physiologically more advantageous extracellular location enabling, through H_2O_2 production, use of the enzyme in external mechanisms for the recovery of nutritional resources from decayed wood. The proposed modification resulting in putative PTS3 of methylotrophic yeasts is apparently missing from the *G. trabeum* AOX sequence.

As expected, the N-terminal region of the *G. trabeum* AOX sequence contains the common ADP-binding motif ($\beta\alpha\beta$) present in most FAD-binding proteins containing the characteristic nucleotide-binding site GxGxxG, specifically GGGPAG for amino acids 13 to 18, which compares with the corresponding sequence GGGSTG (amino acids 13 to 18) of yeast AOXs (44, 57). Other conserved sequence regions of the FAD-binding domain that are found in flavoproteins of the glucose-methanol-choline oxidoreductase family are also present (not shown). The sequence of the enzyme includes two theoretical N-glycosylation sites conforming to the consensus N-X-S/T sequence for Asn residues at positions 141 and 323, both being predicted by the NetNGlyc 1.0 server (www.cbs.dtu.dk/services/NetNGlyc) to be modified with only low N-glycosylation potential (0.399 and 0.545). This is in accord with negative staining for AOX's glycomoiety using the dansyl hydrazine method.

Ultrastructural localization. In yeasts, AOX activity is regulated at the transcriptional level by repression and/or derepression (44). The enzyme is synthesized as an inactive monomer in the cytosol and posttranslationally imported into peroxisomes, where the active homo-octameric FAD-containing enzyme is assembled (20). Ultrastructural localization of AOX in basidiomycete fungi has not been demonstrated to date. Here we present a marked difference in ultrastructural localization of *G. trabeum* AOX compared to the methylotrophic yeasts, the enzyme in this fungus being apparently translocated to the periplasmic and extracellular space. During our TEM labeling studies we were, however, unable to localize *G. trabeum* AOX in peroxisomes, a result consistent with the molecular studies.

Immunofluorescence and TEM-immunogold labeling studies showed AOX to be associated with *G. trabeum* hyphal cell walls (periplasmic space and intrahyphal spaces), extracellular slime, and tripartite membranes emanating from hyphae. This was shown for agitated liquid cultures at different stages of AOX production and on degraded birch and pine wood blocks and on cotton fibers. Immunofluorescence provided a broad overview of positive AOX labeling on hyphal walls and extracellular slime present in pellets and with hyphae growing on cotton fibers or in wood fibers at different stages of decay. AOX has been previously reported from yeasts, fungi imperfecti, and white rot fungi (44), but an extracellular distribution of the enzyme has not been reported previously for fungi. The exception is a structurally unrelated extracellular AOX recently isolated from the thermophilic ascomycete fungus *Thermoascus aurantiacus* and characterized as a heterooctameric flavoglycoprotein composed of two types of subunits, oxidizing in addition to primary aliphatic alcohols also secondary and aromatic alcohols (36).

Implications for wood decay. One of the most important aspects for improved understanding of brown rot decay of wood is knowledge on the involvement and spatial distribution(s) of polysaccharide-degrading agents, including enzymes and nonenzymatic systems in situ. Since the known polysaccharide-degrading enzymes produced by brown rot fungi are considered too large to explain the rapid penetration and attack of wood cell wall components distant to luminal hyphae in wood cells, several systems based on low-molecular-weight active chemicals have been proposed and reviewed recently by Goodell (18). However, in order for these systems to operate in situ, an extracellular source of H_2O_2 is required.

A possible role of AOX as a source of H_2O_2 used in fungal wood decay has already been suggested previously for this enzyme purified from the white rot fungus *P. chrysosporium*

(14, 43). The enzyme was, however, considered an intracellular protein, which was controversial for its implication in fungal decay processes. Extracellular localization of AOX in our present study thus underlines the possible role of AOX to serve as an important extracellular source of H_2O_2 during brown rot and perhaps also white rot decay. The enzyme may thus significantly contribute to the efficiency of the Fenton chemistry for production of highly biodegradative ·OH radicals in degraded wood.

Apparently controversial to the proposed role in wood decay is the instability of AOX at acidic pH conditions that are characteristic of brown rot wood decay. Although this is true for the soluble purified enzyme, its localization in the periplasmic space and "immobilization" in the hyphal polysaccharide sheath may account for the enzyme's physiological functionality, providing the fungus can control pH at the hyphal surface and keep it close to neutral (e.g., through oxalate decarboxylation or neutralization in the form of crystalline calcium oxalate, often observed along hyphae). A possible pH gradient may even have a physiological role in preventing hyphae from damage by active radical species formed at low pHs while suppressed at higher pHs in close proximity of hyphae due to higher rate of ferrous auto-oxidation (52). This assumption is contrary to the model of a reciprocal protective pH gradient for hyphae proposed for the brown rot (*Coniophora puteana*) mechanism by Hyde and Wood (28) assuming a pH as low as 2 at the hyphal surface. Furthermore, it is highly possible that the actual pH along a particular hypha growing in wood need not necessarily be constant. For example, it may be first low at the actively growing apical part as the hypha acidifies its environment by oxalate secretion and then become higher when the specific part is aging. There is also considerable variability in the decay environment, since some brown rot fungi strongly reduce the pH of the substrate (e.g., *Postia* spp.), while other species such as the *G. trabeum* used in our study retain wood at a slightly acidic pH (50).

The second reaction product of AOX with methanol, toxic formaldehyde, can either undergo (in hydrated form) subsequent oxidation by the same enzyme (11) thus producing additional H_2O_2, or be oxidized by ·OH radicals from the Fenton reaction to $\cdot HC(OH)_2$, which can subsequently interact with molecular oxygen (39). In this way (possibly together with other enzymes acting on formaldehyde intracellularly), its accumulation at toxic concentrations deleterious to the fungus may be prevented.

The present results also indicate that the association of AOX with secreted extracellular membranous or slime structures could provide a means for transporting a high molecular enzyme to sites of attack remote from hyphae, i.e., on the lumen wall of degraded wood cells. In addition, AOX associated this way with hyphal cell walls will have direct contact with the substrate, as will hyphae growing within or "sunken" into the secondary wood cell wall (Fig. 8B). We have previously shown the association of another H_2O_2-producing high-molecular-weight (~300 kDa) oxidoreductase, pyranose 2-oxidase (EC 1.1.3.10), with extracellular slime during the decay of wood by the white rot fungi *P. chrysosporium*, *Trametes versicolor*, and *Oudemansiella mucida* (7). This enzyme is also synthesized by *G. trabeum* (our unpublished observations) and may function in the production of active oxygen species synergistically with AOX. Extracellular glyoxal oxidase suggested as a major possible source of H_2O_2 for fungal (*P. chrysosoporium*) lignocellulolytic activities (33) has not yet been reported with *G. trabeum*.

As an enzyme-protein "supporting" matrix, extracellular slime in its various forms, such as sheaths, mycofibrils, and tripartite membranes, has been shown associated with most types of fungal and bacterial wood decay (6, 17, 22, 26, 46), including basidiomycete fungi. It was shown to be associated in the white rot decay of lignocellulose with ligninolytic peroxidases (6, 10, 46) and laccase (9, 42), as well as aryl-alcohol oxidase (2). Thus, a similar role of a functional matrix for the slime in *G. trabeum*, a fungus known to produce extracellular sheaths during degradation of cellulose (26), would seem reasonable. From TEM-immunogold labeling it was, however, not possible to determine whether AOX was located directly on the tripartite membranes or associated with the more electron-dense slime materials bound to its structure. Previous studies on the chemical composition of tripartite membranes from *Sporotrichum pulverulentum* have shown the presence of several proteins of different molecular weights (17). Other studies have shown a monokaryotic strain of the brown rot fungus *Postia placenta* that lost production of extracellular slime unable to degrade wood (40).

A better understanding of AOX's molecular and genetic properties and its involvement in oxidative wood degradation by *G. trabeum* increases our knowledge of the principles underlying brown rot decay. Through finding the enzyme's specific inhibitors, an aspect currently under study, it may further help in the development of targeted wood preservatives.

Conclusions. These new findings in support of the role of AOX in brown rot decay of wood by *G. trabeum* include (i) the extracellular nature of *G. trabeum* AOX, as shown by the enzyme's periplasmic distribution and localization on secreted tripartite membranes and slime materials; (ii) a unique AOX C-terminal sequence that does not contain a signal for peroxisomal targeting, in accord with finding i; and (iii) the high activities of AOX in liquid cultures, which are consistent with a major metabolic role for the enzyme. Finally, methanol, the preferred AOX substrate, is available through its production during concomitant lignin demethylation (thus, a coupling between cellulose and lignin biotransformation is possible).

ACKNOWLEDGMENTS

This study was supported by the Swedish Council for Environment, Agriculture, and Spatial Planning (FORMAS) (2004-1850) and Institutional Research Concept No. AV0Z50200510 (Czech Republic).

REFERENCES

1. **Ander, P., and K. E. Eriksson.** 1985. Methanol formation during lignin degradation by *Phanerochaete chrysosporium*. Appl. Microbiol. Biotechnol. **21:**96–102.
2. **Barrasa, J. M., A. Gutiérrez, V. Escaso, F. Guillén, M. J. Martinez, and A. T. Martinez.** 1998. Electron and fluorescence microscopy of extracellular glucan and aryl-alcohol oxidase during wheat-straw degradation by *Pleurotus eryngii*. Appl. Environ. Microbiol. **64:**325–332.
3. **Bringer, S., B. Sprey, and H. Sham.** 1979. Purification and properties of alcohol oxidase from *Poria contigua*. Eur. J. Biochem. **101:**563–570.
4. **Canton, F. R., M. F. Suarez, M. Jose-Estanyol, and F. M. Canovas.** 1999. Expression analysis of a cytosolic glutamine synthetase gene in cotyledons of Scots pine seedlings: developmental, light regulation and spatial distribution of specific transcripts. Plant Mol. Biol. **40:**623–634.
5. **Cohen, R., M. R. Suzuki, and K. E. Hammel.** 2004. Differential stress-induced regulation of two quinone reductases in the brown-rot basidiomycete *Gloeophyllum trabeum*. Appl. Environ. Microbiol. **70:**324–331.

6. **Daniel, G.** 1994. Use of electron microscopy for aiding our understanding of wood biodegradation. FEMS Microbiol. Rev. **13:**199–233.
7. **Daniel, G., J. Volc, and E. Kubátová.** 1994. Pyranose oxidase, a major source of H_2O_2 during wood degradation by *Phanerochaete chrysosporium*, *Trametes versicolor*, and *Oudemansiella mucida*. Appl. Environ. Microbiol. **60:**2524–2532.
8. **Daniel, G., J. Volc, E. Kubátová, and T. Nilsson.** 1992. Ultrastructural and immunocytochemical studies on the H_2O_2-producing enzyme pyranose oxidase in *Phanerochaete chrysosporium* grown under liquid culture conditions. Appl. Environ. Microbiol. **58:**3667–3676.
9. **Daniel, G., J. Volc, and M.-L. Niku-Paavola.** 2004. Cryo-FE-SEM and TEM immuno-techniques reveal new details for understanding white rot decay of lignocellulose. C. R. Biol. **327:**861–871.
10. **Daniel, G., T. Nilsson, and B. Pettersson.** 1989. Intra- and extracellular localization of lignin peroxidase during degradation of solid wood and wood fragments by *Phanerochaete chrysosporium* by using transmission electron microscopy and immunogold labeling. Appl. Environ. Microbiol. **55:**871–881.
11. **Danneel, H.-J., A. Reichert, and F. Giffhorn.** 1994. Production, purification and characterization of an alcohol oxidase of the ligninolytic fungus *Peniophora gigantea*. J. Biotechnol. **33:**33–41.
12. **Eckhardt, A. E., C. E. Hayes, and J. Goldstein.** 1976. A sensitive fluorescent method fort he detection of glycoprotein in polyacrylamide gels. Anal. Biochem. **73:**192–197.
13. **Enoki, A., S. Itakura, and H. Tanaka.** 1997. The involvement of extracellular substances for reducing molecular oxygen to hydroxyl radical and ferric iron to ferrous iron in wood degradation by wood decay fungi. J. Biotechnol. **53:**265–272.
14. **Eriksson, K. E., and A. Nishida.** 1988. Methanol oxidase of *Phanerochaete chrysosporium*. Methods Enzymol. **161:**322–326.
15. **Eriksson, K.-E., R. A. Blanchette, and P. Ander.** 1990. Microbial and enzymatic degradation of wood and wood components, p. 407. *In* Springer series in wood science. Springer, Berlin, Germany.
16. **Filley, T. R., G. D. Cody, B. Goodell, J. Jellison, C. Noser, and A. Ostrofsky.** 2002. Lignin demethylation and polysaccharide decomposition in spruce sapwood degraded by brown rot fungi. Org. Geochem. **33:**111–124.
17. **Foisner, R., K. Messner, H. Stachelberger, and M. Röhr.** 1985. Wood decay by basidiomycetes: extracellular tripartite membranous structures. Trans. Br. Mycol. Soc. **85:**257–266.
18. **Goodell, B.** 2003. Brown-rot fungal degradation of wood: our evolving view, p. 97–119. *In* B. Goodell, D. D. Nicholas, and T. P. Schultz (ed.), Wood deterioration and preservation: advances in our changing world. ACS series 845. ACS, Washington, DC.
19. **Goodell, B., J. Jellison, J. Liu, G. Daniel, A. Paszczynski, F. Fekete, S. Krishnamurty, L. Jun, and G. Xu.** 1997. Low molecular weight chelators and phenolic compounds isolated from wood decay and their role in the fungal biodegradation of wood. J. Biotechnol. **53:**133–162.
20. **Goodman, J. M., C. W. Scott, P. W. Donahue, and J. P. Atheron.** 1984. Alcohol oxidase assembles post-translation all into the peroxisome of *Candida boidinii*. J. Biol. Chem. **259:**8485–8493.
21. **Green, F., and T. L. Highley.** 1997. Mechanism of brown rot decay: paradigm or paradox. Int. Biodeter. Biodegr. **39:**113–124.
22. **Green, F., M. J. Larsen, L. Murmanis, and T. L. Highley.** 1992. Immunoscanning electron microscopic localization of extracellular polysaccharidases within the fibrillar sheath of the brown rot fungus *Postia placenta*. Can. J. Bot. **38:**898–904.
23. **Gunkel, K., R. van Dijk, M. Veenhuis, and I. J. van der Klei.** 2004. Routing of *Hansenula polymorpha* alcohol oxidase: an alternative peroxisomal protein-sorting machinery. Mol. Biol. Cell **15:**1347–1355.
24. **Hallivell, B., and J. M. C. Gutteridge.** 1999. Free radicals in biology and medicine, 3rd ed. Oxford University Press, Oxford, United Kingdom.
25. **Hammel, K. E., R. Cohen, and M. R. Suzuki.** 2004. Biodegradative activities expressed by the brown rot basidiomycete *Gloeophyllum trabeum* on crystalline cellulose, p. 87–88. Ninth International Conference on Biotechnology in the Pulp and Paper Industry, Durban, South Africa.
26. **Highley, T. L., L. Murmanis, and J. G. Palmer.** 1983. Electron microscopy of cellulose decomposition by brown rot fungi. Holzforschung **37:**271–277.
27. **Holzmann, K., E. Schreiner, and H. Schwalb.** 2002. A *Penicillium chrysogenum* gene (*aox*) identified by specific induction upon shifting pH encodes for a protein which shows high homology to fungal alcohol oxidases. Curr. Genet. **40:**339–344.
28. **Hyde, S. M., and P. Wood.** 1997. A mechanism for production of hydroxyl radicals by the brown-rot fungus *Coniophora puteana*: Fe(III) reduction by cellobiose dehydrogenase and Fe(II) oxidation at a distance from the hyphae. Microbiology **143:**259–266.
29. **Janssen, F. W., and W. Ruelius.** 1968. Alcohol oxidase, a flavoprotein from several basidiomycete species: crystallization by fractional precipitation with polyethylene glycol. Biochim. Biophys. Acta **151:**330–342.
30. **Jensen, Jr., K. A., C. J. Houtman, Z. C. Ryan, and K. E. Hammel.** 2001. Pathways for extracellular Fenton chemistry in the brown rot basidiomycete *Gloeophyllum trabeum*. Appl. Environ. Microbiol. **67:**2705–2711.
31. **Jensen, K. A., Jr., Z. C. Ryan, A. V. Wymelenberg, D. Cullen, and K. E. Hammel.** 2002. An NADH:quinone oxidoreductase active during biodegradation by the brown-rot basidiomycete *Gloeophyllum trabeum*. Appl. Environ. Microbiol. **68:**2699–2703.
32. **Kerem, Z., K. A. Jensen, Jr., and K. E. Hammel.** 1999. Biodegradative mechanisms of the brown rot basidiomycete *Gloeophyllum trabeum*: evidence for an extracellular hydroquinone-driven Fenton reaction. FEBS Lett. **446:**49–54.
33. **Kersten, P. J., and D. Cullen.** 1993. Cloning and characterization of a cDNA encoding glyoxal oxidase, a H_2O_2-producing enzyme from the lignin-degrading basidiomycete Phanerochaete chrysosporium. Proc. Natl. Acad. Sci. USA **90:**7411–7413.
34. **Kerwin, R. M., and H. W. Ruelius.** 1969. Production of alcohol oxidase by several basidiomycetes. Appl. Microbiol. **17:**347–351.
35. **Kirk, T. K., R. Ibach, M. D. Mozuch, A. H. Conner, and T. L. Highley.** 1991. Characteristics of cotton cellulose depolymerized by a brown-rot fungus, by acid, or chemical oxidants. Holzforschung **45:**230–244.
36. **Ko, H.-S., Y. Yokoyama, N. Ohno, M. Okadome, S. Amachi, H. Shinoyama, and T. Fujii.** 2005. Purification and characterization of intracellular and extracellular, thermostable and alkali-tolerant alcohol oxidases produced by a thermophilic fungus, *Thermoascus aurantiacus* NBRC 31693. J. Biosci. Bioeng. **99:**348–353.
37. **Koenigs, J. W.** 1974. Hydrogen peroxide and iron: a proposed system for decomposition of wood by brown-rot basidiomycetes. Wood Fiber Sci. **6:**66–79.
38. **Ledeboer, A. M., L. Edens, J. Maat, C. Visser, J. W. Bos, and C. T. Verrips.** 1985. Molecular cloning and characterization of a gene coding for methanol oxidase in *Hansenula polymorpha*. Nucleic Acids Res. **13:**3063–3082.
39. **Merz, J. H., and W. A. Waters.** 1949. Some oxidations involving the free hydroxyl radical. J. Chem. Soc. **1949:**15S–25S.
40. **Micales, J. A., A. L. Richter, and T. L. Highley.** 1990. Extracellular glucan production by *Postia* (=*Poria*) *placenta*. Mater. Org. **24:**259–269.
41. **Newcombe, D., A. Paszczynski, W. Gajewska, M. Kroger, G. Feis, and R. Crawford.** 2002. Production of small molecular weight catalysts and the mechanism of trinitrotoluene degradation by several *Gloeophyllum* species. Enzyme Microb. Technol. **30:**506–517.
42. **Nicole, M., H. Chamberland, D. Rioux, N. Lecours, B. Rio, J. P. Geiger, and G. B. Quellette.** 1993. A cytochemical study of extracellular sheaths associated with *Rigidoporus lignosus* during wood decay. Appl. Environ. Microbiol. **59:**2578–2588.
43. **Nishida, A., and K.-E. Eriksson.** 1987. Formation, purification and partial characterization of methanol oxidase, a H_2O_2-producing enzyme in *Phanerochaete chrysosporium*. Biotechnol. Appl. Biochem. **9:**325–338.
44. **Ozimek, P., M. Veenhuis, and I. J. van der Klei.** 2005. Alcohol oxidase: a complex peroxisomal, oligomeric flavoprotein. FEMS Yeast Res. **5:**975–983.
45. **Paszczynski, A., R. Crawford, D. Funk, and B. Goodell.** 1999. De novo synthesis of 4,5-dimethoxycatechol and 2,5-dimethoxyhydroquinone by the brown rot fungus *Gloeophyllum trabeum*. Appl. Environ. Microbiol. **65:**674–679.
46. **Ruel, K., and J.-P. Joseleau.** 1991. Involvement of an extracellular glucan sheath during degradation of *Populus* wood by *Phanerochaete chrysosporium*. Appl. Environ. Microbiol. **57:**374–384.
47. **Schlosser, D., K. Fahr, W. Karl, and H.-G. Wetzstein.** 2000. Hydroxylated metabolites of 2,4-dichlorophenol imply a Fenton-type reaction in *Gloeophyllum striatum*. Appl. Environ. Microbiol. **66:**2479–2483.
48. **Segers, G., N. Bradshaw, D. Archer, K. Blissett, and R. P. Oliver.** 2001. Alcohol oxidase is a novel pathogenicity factor for *Cladosporium fulvum*, but aldehyde dehydrogenase is dispensable. Mol. Plant-Microbe Interact. **14:**367–377.
49. **Soldevila, A. I., and S. A. Ghabrial.** 2001. A novel alcohol oxidase/RNA-binding protein with affinity for mycovirus double-stranded RNA from the filamentous fungus *Helminthosporium* (*Cochliobolus*) *victoriae*: molecular and functional characterization. J. Biol. Chem. **276:**4652–4661.
50. **Suzuki, M. R., C. G. Hunt, C. J. Houtman, Z. D. Dalebroux, and K. E. Hammel.** 2006. Fungal hydroquinones contribute to brown rot of wood. Environ. Microbiol. **8:**2214–2223.
51. **Szamecz, B., G. Urbán, R. Rubiera, J. Kucsera, and L. Dorgai.** 2005. Identification of four alcohol oxidases from methylotropic yeasts. Yeast **22:**669–676.
52. **Varela, E., and M. Tien.** 2003. Effect of pH and oxalate on hydroquinone-derived hydroxyl radical formation during brown rot wood degradation. Appl. Environ. Microbiol. **69:**6025–6031.
53. **Wang, W., and P. J. Gao.** 2002. A peptide-mediated and hydroxyl radical HO·-involved oxidative degradation of cellulose by brown-rot fungi. Biodegradation **13:**383–394.
54. **Wang, W., and P. J. Gao.** 2003. Function and mechanism of a low-molecular-weight peptide produced by *Gloeophyllum trabeum* in biodegradation of cellulose. J. Biotechnol. **101:**119–130.
55. **Waterham, H. R., K. A. Russell, Y. Vries, and J. M. Cregg.** 1997. Peroxisomal targeting, import, and assembly of alcohol oxidase in *Pichia pastoris*. J. Cell Biol. **139:**1419–1431.
56. **Werner, W., H. G. Rey, and H. Z. Wielinger.** 1970. Über die Eigenschaften

eines neuen Chromogens für die Blutzuckerbestimmung nach der GOD/POD Methode. Z. Anal. Chem. **252:**224–228.
57. **Wierenga, R. K., P. Terpstra, and W. G. Hol.** 1986. Prediction of the occurrence of the ADP-binding βαβ-fold in proteins, using an amino acid sequence fingerprint. J. Mol. Biol. **187:**101–107.
58. **Xu, G., and B. Goodell.** 2001. Mechanisms of wood degradation by brown-rot fungi: chelator-mediated cellulose degradation and binding of iron by cellulose. J. Biotechnol. **87:**43–57.
59. **Yphantis, D. A.** 1964. Equilibrium ultracentrifugation of dilute solutions. Biochemistry **3:**297–317.
60. **Yomo, T., I. Urabe, and H. Okada.** 1989. Enzymatic method for measuring the absolute values of oxygen concentration. Anal. Biochem. **179:**124–126.